Proceedings of HT2007
2007 ASME-JSME Thermal Engineering Summer Heat Transfer Conference
July 8-12, 2007, Vancouver, British Columbia, CANADA

DRAFT - HT2007-32618

ON CORRELATING EXPERIMENTAL PRESSURE FLOW AND HEAT TRANSFER MEASUREMENTS FROM SILICON MICROCHANNELS WITH THEORETICAL CALCULATIONS

Cormac Eason[1] **Niall O'Keeffe**[1]

Ryan Enright[1] [1]Stokes Research Institute, University of Limerick, Co. Limerick, Ireland cormac.eason@ul.ie **Tara Dalton**[1]

ABSTRACT

The bulk pressure flow and heat transfer characteristics of rectangular and trapezoidal microchannels etched in silicon were measured in the laminar regime. The channel hydraulic diameters were 305 µm for the Deep Reactive Ion Etched (DRIE) etched channel and 317 µm for the wet etched channel and there were 22 channels in each sample. The fluid used was purified degassed water.

The inlet and outlet temperature and pressure of the fluid and the wall temperatures of the channels were measured at the inlet and outlet of the channels. Theoretical and experimental results were calculated using fluid properties at the mean fluid temperature for each data point. These were then collapsed to a single curve at constant temperature by multiplying the measured value by the ratio of the relevant fluid properties at the experimental and required temperatures.

The cross section of each channel on each channel sample was measured along with the channel height and width to give an area ratio between the actual channel width and the width calculated assuming the channel was perfectly rectangular or trapezoidal. This ratio is used to compensate the theoretical results and improve their correlation with the experiment.

The uncertainty in the experimental results was calculated by running the result processing calculations three times, once at nominal values and then shifting input values to their upper and lower limits based on a 95% confidence interval on the standard deviation for each inputted measurement.

Theoretical calculations were run for each experimental mass flow rate in order to produce equivalent theoretical points to the experimental values. Uncertainty in the theory is also determined by running the theoretical calculations at upper, lower and nominal 95% confidence interval values for the channels being tested.

It was found that while the pressure flow data from the channels matched theoretical trends and that the results for the rectangular DRIE channels showed no experimentally significant deviation from theory, the experimental data from the wet etched trapezoidal channels was lower than predictions.

The heat transfer from the channels is strongly affected by the heat transferred to the coolant by the manifolds. When this effect is removed, the experimental Reynolds number Nusselt number plot becomes strongly linear. This does not agree with theoretical predictions.

NOMENCLATURE

Symbol	Description	Unit
A	Channel cross sectional area (CSA)	m^2
A_M	Manifold CSA/Number of channels (n)	m^2
$B_{1,2}, C_{1\text{-}4}, \lambda$	Constants for Calculation[13]	No Unit
D_h	Hydraulic diameter	m
H	Channel height	m
L	Channel Length	m
M	Blending parameter $M = 2.27 + 1.65Pr$	No Unit
Nu	Average Nusselt number = hD_h/k	No Unit
P_L	Pressure drop along channel	Pa
Pr	Prandtl number ($\mu c_p/k$)	No Unit
Re	Reynolds number $\frac{\rho u D_h}{\mu}$	No Unit
$Re_{\sqrt{A}}$	Reynolds number $\frac{\rho u \sqrt{A}}{\mu}$	No Unit
T	Temperature	°C

W	Channel width	m
W_b	Width of base of trapezoidal channel	m
c_p	Specific heat capacity	J/kgK
f	Friction factor	No Unit
$f(Pr)$	Friction factor for variation in Pr	No Unit
h	Average convection heat transfer	W/m2K
k	Coolant conductivity	W/mK
$\dot{m}$	Mass flow rate	kg/s
n	Number of channels	No unit
u	Mean fluid velocity	m/s
z^+	Dimensionless Length $z^+ = \frac{L}{\sqrt{A}\,Re_{\sqrt{A}}}$	No Unit
z^*	Dimensionless Length $z^* = z^+/Pr$	No Unit

Greek Letters

ε	Channel aspect ratio W/H	No Unit
μ	Fluid viscosity	Pa s
ρ	Fluid density	kg/m3
ϕ	Trapezoidal channel sloped wall angle	Degrees

Subscripts

Avg	Average value
Comp	Area compensated
Exp	Experimentally measured value
F	Property of fluid
M	Property of manifold
Muzy	Muzychka and Yovanovich correlation[13]
S	Property of microchannel surface
Theory	Value calculated theoretically
exp	Experimentally measured value
i	Inlet manifold/state
in	State at channel inlet
o	Outlet manifold/state
out	State at channel outlet

INTRODUCTION

The pressure flow and heat transfer behaviour of fluids in microchannels is an area in which there remains considerable disagreement between classical theoretical correlations and experimental measurements, even in the area of laminar flow. Steinke and Kandlikar[17] compiled 220 sets of data for single phase flow in microchannels between 1 and 1200 microns in diameter and reported experimental data varying over approximately an order of magnitude around theoretical laminar flow values. Garimella[8] also plotted pressure flow data from microchannels from several researchers, showing the same trend of inconsistency in friction factors from paper to paper.

While certain of the inconsistencies in these measurements are related to micro and nano scale effects such as the electric double layer, loss of the continuum assumption validity due to small length scales and compressibility effects or other fluid property changes along the channel, in many cases the lack of correlation between theory and result is more likely to be related to the inherent difficulties in taking measurements from flows at this scale combined with high uncertainties in results derived from experimental measurements[9].

Heat transfer from microchannels is again an area in which wide variation between conventional theory and experimental results can be seen. Garimella in [8] plots a wide variety of Reynolds number Nusselt number correlations measured over the past 15 years. Recent work measuring local heat transfer from microchannels using liquid crystal thermography showed good correlation between laminar theory and experimental data however[12], so the possibility of agreement remains.

Work by Bavière et al[1] found that for a parallel plate channel once bias effects in the measurement of the channel surface temperature and fluid temperature were accounted for that the test channel results correlated with conventional heat transfer laws in both the laminar and turbulent regimes.

The use of numerical simulation for heat transfer in developing laminar flows has also produced good correlation with experimental data in work by Lee and Garimella[10], and Tiselj et al[18] indicating that while standard correlations may not be adequate for certain situations, numerical simulation can correlate well with experimental data for specific test systems.

Work by Shen et al.[16] found that the inlet coolant temperature affected the heat transfer performance from a microchannel system while measuring Nusselt numbers significantly below theoretical predictions. The Nusselt number was noted to increase with the Reynolds number however.

This work experimentally measures the bulk pressure flow and heat transfer behaviour for arrays of rectangular and trapezoidal silicon microchannels, both measured using the same modular microchannel test system. Corresponding theoretical values are calculated for each experimental data point measured using accepted correlations for macro scale laminar flow and heat transfer. The cross sectional area of the channels was measured using a digital camera attached to an optical microscope and is used to further refine the theoretical calculation as the channels are not the perfectly rectangular or trapezoidal shapes the correlations describe.

Uncertainty in the theoretical calculations is found by recalculating all data points at the upper and lower bounds of a 95% confidence interval on the measured dimensions of the channels. Uncertainty in the experimental measurements is found based on the apparatus uncertainty or the cumulative uncertainty where values are derived.

EXPERIMENTAL DESCRIPTION

A test system was built to circulate water through an array of microchannels, supply heat to the channels and measure the heat transfer from, pressure drop across and mass flow through the channels. A schematic of this system can be seen in Figure 1, while a CAD drawing of the microchannel manifold is shown in Figure 2. The components used to build the system are described as follows:

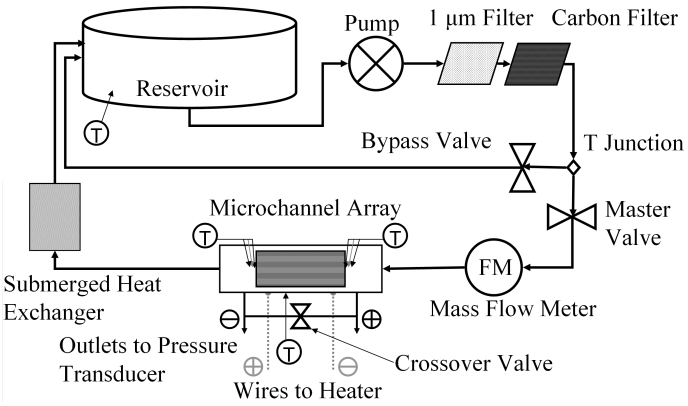

FIGURE 1: SCHEMATIC OF TEST SYSTEM. ENCIRCLED 'T'S INDICATE THERMOCOUPLE LOCATIONS

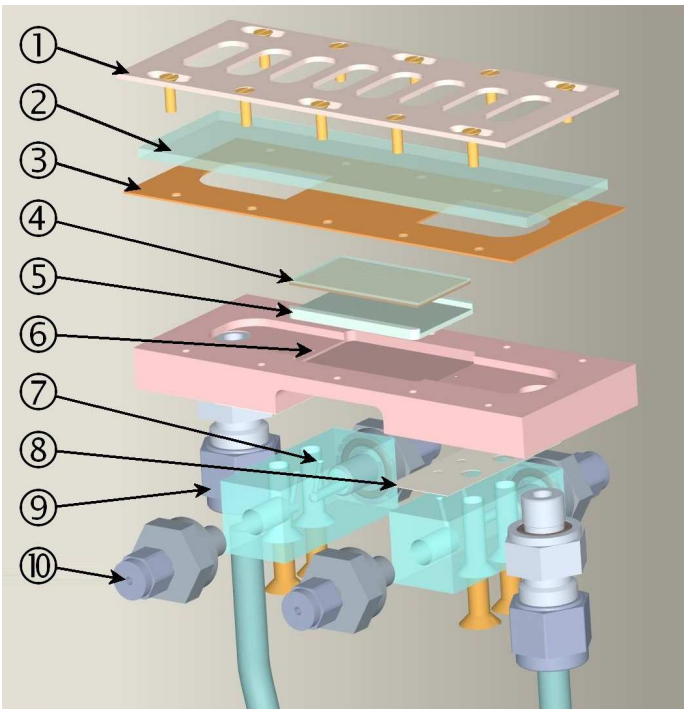

FIGURE 2: DETAIL OF MICROCHANNEL ARRAY: 1. COVER PLATE, 2. GLASS SLIDE, 3. GASKET MADE FROM A DOUBLE LAYER OF SILICONE RUBBER, 4. MICROCHANNEL SAMPLE, 5. ALUMINIUM SPACING SHIM, 6. PRESSURE TAPPING IN ALUMINIUM MANIFOLD BLOCK, 7. PRESSURE TAPPING MANIFOLD (HEATERS FITTED TO MANIFOLD BLOCK BETWEEN MANIFOLDS), 8. MANIFOLD GASKET MADE FROM PTFE, 9. INLET TUBING CONNECTION COMPRESSION FITTING, 10. COMPRESSION FITTING TO CONNECT PRESSURE TRANSDUCER.

Pumping

The fluid is pumped through the system using a speed controlled Tuthill pump motor (V2DC00S00000) magnetically coupled to a gear pump (DDS.19PPPV2NM00000) displacing 0.19 ml per revolution. The pump motor can run at speeds from 60 to 3600 rpm and is load sensing, allowing it to maintain a constant pump speed regardless of the load on the motor.

Filters

A two stage filter stack was used to filter the water flowing through the system. The filters used were a Whatman polycap 36 HD 6703-3610 1 µm filter and a carbon cap 6704-1500 activated carbon filter to remove organic contaminants.

Mass Flow

The mass flow rate is measured with a Bronkhurst liquiflow L30 mass flow meter calibrated to ±1% of its 10 kg/hr (2.78 g/s) maximum flow rate. This flow meter measures the mass flow through the system by measuring how much heat it needs to supply to the fluid flowing through it to maintain a constant temperature rise through the flow meter.

Pressure

Pressure tappings 0.5 mm in diameter were machined at the centre of the inlet and outlet manifolds 1.5 mm from the entrance and exit of the channels. These are connected via a custom made perspex manifold block to a Setra model 2301001PD2F2EBC pressure transducer rated to 6.89 kPa (1 PSI) ±0.25%.

Temperature Measurement

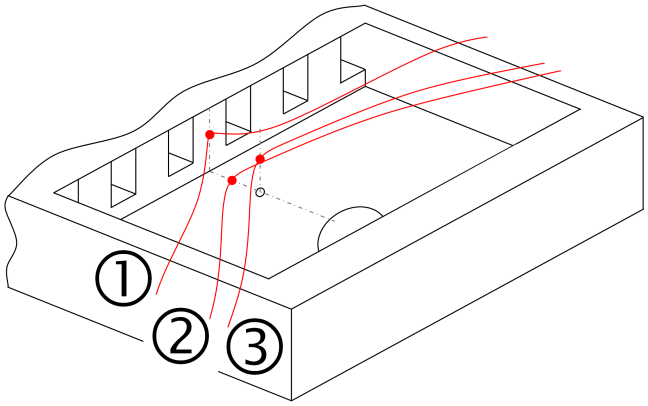

FIGURE 3:THERMOCOUPLE LOCATIONS IN MANIFOLDS; 1: CHANNEL SURFACE TEMPERATURE THERMOCOUPLE AT CENTRE OF WALL BETWEEN CENTRE TWO CHANNELS, 2: MANIFOLD WALL CENTERED BETWEEN PRESSURE TAPPING (OPEN CIRCLE) AND CHANNEL WALL ON CENTRE LINE, 3: WATER TEMPERATURE THERMOCOUPLE, SUSPENDED IN MANIFOLD ABOVE PRESSURE TAPPING. (DIAGRAM NOT TO SCALE).

A thermocouple was mounted in the reservoir and on the heating resistors to detect overheating. Three thermocouples were fitted in each of the inlet and outlet manifolds as shown in Figure 3.

Bare wire Omega CHAL-005 K-Type thermocouples were used to measure temperature data from the manifolds. These

thermocouples have wire diameters of 127 µm and could be run from the manifold between the two layers of rubber gasket without causing leakage from the system. K-Type thermocouples were chosen as the Chromel/Alumel wires from which they are made have low thermal conductivity, reducing the effect of thermal conduction along the thermocouples on the temperature of the surface they're measuring from. The thermocouples were calibrated to ±0.1°C in a temperature controlled water bath regulated by a PID controller and platinum resistance thermometer. The voltages from the thermocouples were amplified using a custom built thermocouple amplifier based on Analog devices AD595 chips.

Heating

The channels were heated using an array of 3 aluminium bodied power resistors (Farnell order 9506861). These were mounted longitudinally to the back of the manifold block between the pressure tapping manifolds (See Figure 2) using a high temperature thermal epoxy.

Data Acquisition

A National Instruments LabVIEW PCI-6251 card was used to control the pump speed as well as to log data from the thermocouples, mass flow meter and pressure transducer. This card logs between -10 and +10 V with a 16 bit accuracy, with indicated output to 1 mV.

LOGGED INFORMATION FROM SYSTEM

- Pressure difference between the Inlet and Outlet of the sample channels – (P_{Lexp}).
- Pump Motor Speed (RPM) – Set from LabVIEW program.
- Power input to the power resistors (W) – Measured from power supply.
- Mass flow rate – ($\dot{m}$).
- Temperatures of inlet and outlet manifold surfaces (°C) – (T_{inM}, T_{outM}).
- Temperatures of inlet and outlet fluid (°C) – (T_{inF}, T_{outF}).
- Temperatures of sample surface at inlet and outlet (°C) – (T_{inS}, T_{outS}).

MICROCHANNEL DESCRIPTION AND DIMENSIONS

Two types of microchannel were tested for this work. The first was etched in silicon using deep reactive ion etching (DRIE) to create 22 parallel rectangular channels across a 15mm width. The second set of channels was created by wet etching silicon using a Potassium Hydroxide (KOH) solution. This produced an array of 22 trapezoidal channels, again across a 15 mm width. The details of the manufacture process and the modular manifold design can be found in [5] and [6].

The widths and heights of the channels were measured using a CCD camera attached to an optical microscope. Points were scaled from the digital microscope images to define the cross section of the channel using a MATLAB program[7]. These points were exported to ProEngineer, a CAD program where they are used to construct a solid model the same shape as the experimental channel. The CAD program was then used to calculate the cross section of the channel. This cross section is used in the area compensation step of the result processing. Channel length L was measured with a digital calipers to ±0.01 mm. Dimensions of the channels with ±1.96 standard deviations (95% confidence interval) on each dimension are given in Table 1.

TABLE 1: MEASURED CHANNEL DIMENSIONS.

	n	*H (µm)*	*W (µm)*	W_b *(µm)*	*L (mm)*	*Pitch (µm)*
DRIE	22	305.88 ±14.15	304.67 ±5.05	N/A	30.02± 0.01	700
KOH	22	413.02 ±10.82	605.19 ±20.2	24.66± 10.1	29.86± 0.01	690

THEORETICAL CALCULATIONS

Two techniques were used to calculate the theoretical behaviour of the channels. The first uses standard fully developed flow correlations for laminar flow through rectangular and trapezoidal channels and is sourced from Rohsenow[14] and based on fanning friction factors used with Darcy's equation. The second technique was described by Muzychka and Yovanovich[13] in 2004 and uses the cross sectional area and the aspect ratio of the channel to calculate combined thermally and hydrodynamically developing pressure flow and heat transfer characteristics of the channel.

Darcy's Equation

TABLE 2: FRICTION FACTORS FOR FULLY DEVELOPED FLOW THROUGH RECTANGULAR CHANNELS[14].

Aspect Ratio	*fRe*	Aspect Ratio	*fRe*
1	14.22708	0.25	18.23278
0.9	14.26098	0.2	19.0705
1/1.2	14.32808	1/6	19.7022
0.8	14.3778	1/7	20.1931
0.75	14.4757	0.125	20.58464
1/1.4	14.56482	1/9	20.90385
0.7	14.60538	0.1	21.16888
2/3	14.71184	1/12	21.58327
0.6	14.97996	1/15	22.01891
0.5	15.54806	0.05	22.47701
0.4	16.3681	0.02	23.3625
1/3	17.08967	0	24
0.3	17.51209		

The Fanning friction factor f is equal to $16/Re$ for fully developed flow through a round channel. Depending on the aspect ratio of a rectangular channel, the numerator of this equation changes as dictated by the Table 2 from Rohsenow[14]. Darcy's equation is given in (1).

$$P_L = f\frac{4L}{D_h}\frac{\rho u^2}{2} \quad (1)$$

Macro scale heat transfer theory states that the Nusselt number remains constant for fully developed laminar flow through a channel. Fully developed Nusselt numbers for rectangular channels heated from three sides are given in Table 3. The assumption that the channels are heated uniformly from three walls can be used because the silicon from which the channels are made is conductive enough to give a temperature gradient of the order of 0.1°C between the top and bottom of the channel when fin theory is applied to the system. This, combined with the thermocouple measuring the channel surface temperature giving an average temperature for the area to which it is fitted, means that the assumption that the channel walls are at a uniform temperature at any point along the flow direction should not affect the outcome of the experiments in a substantive way. The channels are assumed to have a constant heat flux. A linear interpolation is used to calculate *fRe* and *Nu* values intermediate to the tabulated values.

TABLE 3: FULLY DEVELOPED LAMINAR FLOW CONSTANT HEAT FLUX NUSSELT NUMBER DATA FOR RECTANGULAR CHANNELS WITH 3 WALLS HEATED[15].

W/H	*Nu*	*W/H*	*Nu*
0	0	1.43	3.149
0.1	0.538	2	3.539
0.2	0.964	2.5	3.777
0.3	1.312	3.33	4.06
0.4	1.604	5	4.411
0.5	1.854	10	4.851
0.7	2.263	∞	5.385
1	2.712		

For the case of the trapezoidal channels, the *fRe* and *Nu* values are given in Table 4.

TABLE 4: FRICTION FACTORS AND CONSTANT HEAT FLUX NUSSELT NUMBERS FOR FULLY DEVELOPED FLOW THROUGH TRAPEZOIDAL DUCTS[14].

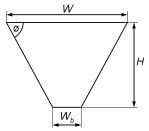

H/Wb	*fRe*	*Nu*
	ø = 85°	
∞	12.474	2.446
8	17.474	4.366
4	16.74	4.483
2	15.015	3.896
4/3	14.312	3.636
1	14.235	3.608
¾	14.576	3.736
½	15.676	4.175
¼	18.297	5.363
1/8	20.599	6.501
0	24	8.235
	ø = 75°	
∞	13.065	2.91
8	14.907	3.52
4	14.959	3.72
2	14.34	3.61
4/3	14.118	3.542
1	14.252	3.594
¾	14.697	3.766
½	15.804	4.219
¼	18.303	5.317
1/8	20.556	6.482
0	24	8.235
	ø = 60°	
∞	13.333	3.111
8	13.867	3.284
4	13.916	3.348
2	13.804	3.35
4/3	13.888	3.39

H/Wb	*fRe*	*Nu*
	ø = 60° (Continued)	
1	14.151	3.495
¾	14.637	3.691
½	15.963	4.14
¼	18.053	5.247
1/8	20.304	6.341
0	24	8.235

H/Wb	*fRe*	*Nu*
	ø = 45°	
∞	13.153	2.982
8	13.301	3.03
4	13.323	3.048
2	13.364	3.081
4/3	13.541	3.155
1	13.827	3.268
¾	14.26	3.469
½	15.206	3.888
¼	17.397	4.943
1/8	19.743	6.034
0	24	8.235
	ø = 30°	
∞	12.744	2.68
8	12.76	2.697
4	12.782	2.704
2	12.875	2.736
4/3	13.012	2.919
1	13.246	2.821
¾	13.599	3.077
½	14.323	3.436
¼	16.284	4.349
1/8	18.479	5.569
0	24	8.235

Muzychka and Yovanovich Correlations

A further correlation for thermally and hydrodynamically developing laminar flow in channels of arbitrary cross sectional area is given in a paper by Muzychka and Yovanovich (2004)[13], which makes use of the square root of the cross sectional area instead of the hydraulic diameter for the channel characteristic dimension. This choice of characteristic dimension was confirmed by the authors of the paper based on results from literature and was found from first principles using constructal theory by Bejan[2]. For a trapezoidal channel the aspect ratio is taken as being the average channel width divided by the channel height.

The friction factor calculation procedure begins with finding the aspect ratio of the channel (Equation (2)). This must be between 0.1 and 1. Parallel plate theory should be used if aspect ratios are below 0.1.

$$\varepsilon = \frac{W}{H} \text{ or } \frac{H}{W},\ 0.1 < \varepsilon < 1 \quad (2)$$

The friction factor times Reynolds number for fully developed flow in a channel was found from Equation (3),

while the apparent friction factor allowing for developing flow effects was found using Equation (4).

$$f\,Re_{\sqrt{A}} = \frac{12}{\sqrt{\varepsilon}(1+\varepsilon)\left[1-\frac{192\varepsilon}{\pi^5}tanh\left(\frac{\pi}{2\varepsilon}\right)\right]} \tag{3}$$

$$f_{app}\,Re_{\sqrt{A}} = \left[\left(f\,Re_{\sqrt{A}}\right)^2 + \left(\frac{3.44}{\sqrt{z^+}}\right)^2\right]^{\frac{1}{2}} \tag{4}$$

A means by which the combined developing Nusselt number for the channels can be calculated is also described[13]. It does not deal with wall heating conditions other than the all walls heated case, but is claimed to work well for both rectangular and trapezoidal channels among others. First the value of $f(Pr)$ is found as in Equation (5). This accounts for the variation in the Prandtl number as the flow develops thermally.

$$f(Pr) = \frac{B_1}{\left[1+\left(B_2\,Pr^{1/6}\right)^{\frac{9}{2}}\right]^{\frac{2}{9}}}, \qquad 0.1 < Pr < \infty \tag{5}$$

The combined developing Nusselt number for the channel is then found by inserting the previously calculated quantities into Equation (6) along with the correct constants from Table 5.

$$Nu_{Muzy} = \left[\left(\frac{C_4 f(Pr)}{\sqrt{z^*}}\right)^M + \left(\left\{C_2 C_3\left(\frac{f\,Re_{\sqrt{A}}}{z^*}\right)^{1/3}\right\}^5 + \left\{C_1\left(\frac{f\,Re_{\sqrt{A}}}{8\sqrt{\pi}\varepsilon^{\lambda}}\right)\right\}^5\right)^{\frac{M}{5}}\right]^{1/M} \tag{6}$$

TABLE 5: CONSTANTS FOR MUZYCHKA AND YOVANOVICH CORRELATION[13].

	B1	*B2*	*C1*	*C3*
Uniform Wall Temp	0.564	1.664	3.24	0.409
Uniform Heat Flux	0.886	1.909	3.86	0.501

	C2	*C4*		λ
Local	1	1	Upper	1/10
Average	3/2	2	Lower	-3/10

Entrance and Exit Losses

Since the pressure tappings are located in the manifolds before and after the channels rather than in the channels themselves, the theoretically calculated pressure drop values must account for the flow friction in the manifolds and the entrance and exit losses caused by the flow constricting at the entrance to and expanding at the exit from the channels. These losses have two components, the reversible loss, based on Bernoulli's equation, and the irreversible losses due to separation and other effects. Data from Rohsenow[14] was used. The formula for calculating the entrance and exit losses is given in Equation (7) using column matrices to distinguish between the inlet pressure drop P_{Li} and the outlet pressure drop P_{Lo}. It should be noted that A_M is the manifold area divided by the number of channels in each sample.

$$\begin{bmatrix} P_{Li} \\ -P_{Lo} \end{bmatrix} = \frac{\rho u^2}{2}\left[\left(1-\left(\frac{A}{A_M}\right)^2\right) + \begin{bmatrix} K_c \\ -K_e \end{bmatrix}\right] \tag{7}$$

K_c and K_e are found using the data in Figure 4

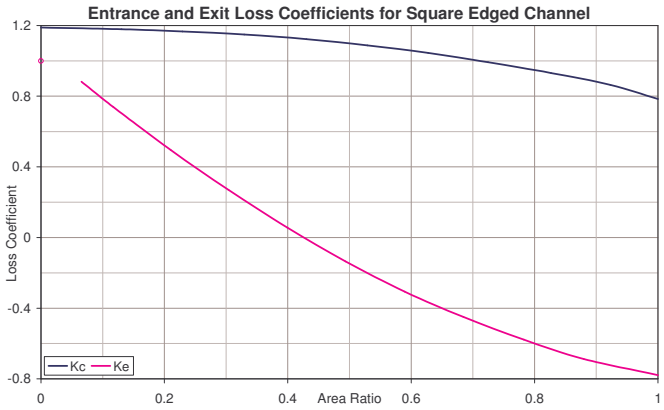

FIGURE 4: EXPANSION AND CONTRACTION LOSS COEFFICIENTS FOR LAMINAR FLOW THROUGH A SQUARE EDGED CONTRACTION OR EXPANSION[14].

EXPERIMENTAL DATA PROCESSING

Data was logged from the test system 4 times a second for 50 samples at each system setting. The system was given a few minutes to reach steady state conditions before data was logged. Each logged data set was averaged in order to eliminate noise in the signal. The standard deviation was taken for each logged data value, multiplied by 1.96 and used as the uncertainty in the measurement of this data. This gives a 95% confidence interval for the measured value. The 95% confidence interval gives a higher magnitude of uncertainty than both the manufacturers' published figures and the calibration uncertainty for the devices used due to the contribution of system noise to the signal. For this reason it gives the most conservative estimate of measurement

uncertainty for each device used in this work. The only exception to this situation was for the temperature measurements for which the calibration bath uncertainty of ±0.1°C was used as it was greater than the standard deviation of the sampled data.

Averaged data was processed using a set of MATLAB programs as described by Eason (2005)[7]. This takes the data on a point by point basis, calculating a theoretical value to correspond with each experimentally measured value. This is necessary, particularly for the heat transfer measurements as the average temperature of the water pumped through the system will vary between data points, leading to changes in the properties of the water and therefore shifts in the theoretical values corresponding with each point compared to a constant temperature theoretical curve. Table 6 shows a summary of the values measured or calculated from the system and their ranges and uncertainties.

TABLE 6: SUMMARY OF UNCERTAINTIES AND EXPERIMENTAL RANGES IN THIS WORK. VALUES MARKED WITH AN ASTERISK ARE MEASURED DIRECTLY.

Measured Value	Range Measured		Max Uncertainty	
Channel Type	DRIE	KOH	DRIE	KOH
Nu	0.065 – 5.73	0.11 – 9.99	±1.33	±0.37
$P_{L(Exp)}$* (Pa)	129.8 – 5679	162.7 – 6094	±24.4	±8.91
Re	4.59 – 168.9	12.1 – 439.2	±10.6	±14.4
T_{outF}-T_{inF} (°C)	0.3 – 19.4	1.8 – 26.6	±0.2	±0.2
T_{outS}-T_{inS} (°C)	1.6 – 20.5	0.8 – 22.2	±0.2	±0.2
T_{outF}* (°C)	26.2 – 63.6	25.9 – 66.7	±0.1	±0.1
h (W/m^2)	1387 – 9680	227 – 19305	±377	±559
$\dot{m}$ * (g/s)	0.038 – 1.63	0.085 – 2.88	±0.01	±0.01

Since the uncertainty for each quantity measured was calculated on a point by point basis, this information is to give a guideline as to the overall system behaviour. Error bars on the result plots show point by point uncertainties.

TEMPERATURE AND AREA COMPENSATION

The theoretical and experimental results are then temperature compensated to produce results at a single temperature by multiplying each value by the ratio of the fluid properties at the experimental temperature and the fluid properties at the target temperature. Only the fluid properties used to derive the required value are used in the normalisation of that value[7]. The correctness of the temperature compensation process chosen is confirmed by the theoretical data points all falling on the same line, rather than just points taken at a particular average fluid temperature falling on the same line as occurs with the uncompensated data.

Equation (8) shows the area compensation as applied to the theoretical pressure drop as calculated using Darcy's equation (1). P_L calculated theoretically is proportional to $1/(AD_h^2) \approx 1/A^2$ when the fRe and $\dot{m}$ values inputted to find the theoretical P_L are substituted into Equation (1). Experimentally measured values are compensated for temperature only as it is implicit in measuring the pressure directly from the experimental system that the pressure drop will already be area compensated.

$$P_{L_{Comp}} = \frac{P_{L_{Theory}}}{\left(A_{Exact} / A_{Theory} \right)^2} \tag{8}$$

MANIFOLD HEATING EFFECT

Since it was not possible to measure the liquid temperature at the entrance to the channels without blocking flow into the channels it was necessary to measure the fluid inlet and outlet temperature away from the channel entrance and exit. For this reason the heating effect of the inlet and outlet manifolds had to be calculated and subtracted from the overall heat transfer measured from the system based on the fluid temperature rise.

The process for calculating the heat transfer from the manifolds was the same as was applied to the rectangular channels, using the data from Table 3 and the Muzychka and Yovanovich correlation to find theoretical Nusselt numbers for the manifolds. The heat transferred by the manifolds was calculated theoretically based on the experimental manifold and fluid temperatures and from this theoretical temperatures for the fluid at the point at which it enters and leaves the channels were found. These temperatures were used to calculate the experimental Nusselt number from the channels.

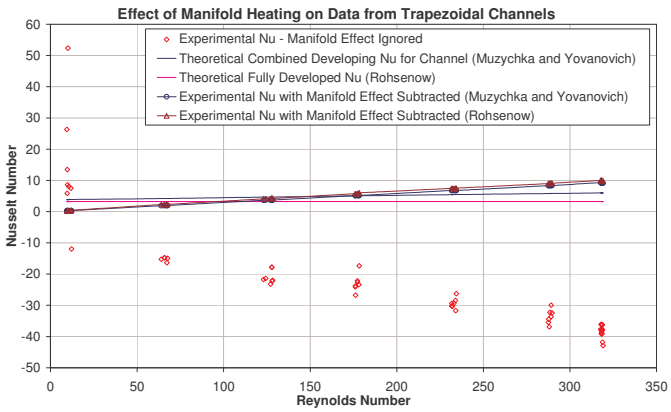

FIGURE 5: EFFECT OF MANIFOLD HEATING ON EXPERIMENTAL NUSSELT NUMBER.

It can be seen from Figure 5 that when the experimental data was processed without the manifold heating effect, the Nusselt numbers measured from the system appeared chaotic and were mostly negative. Once the manifold heating is applied, using either the Muzychka and Yovanovich[13] or the Rohsenow[14] correlation to predict the heat transfer from the manifolds however, the experimental data falls onto a straight line.

RESULTS

Pressure flow data

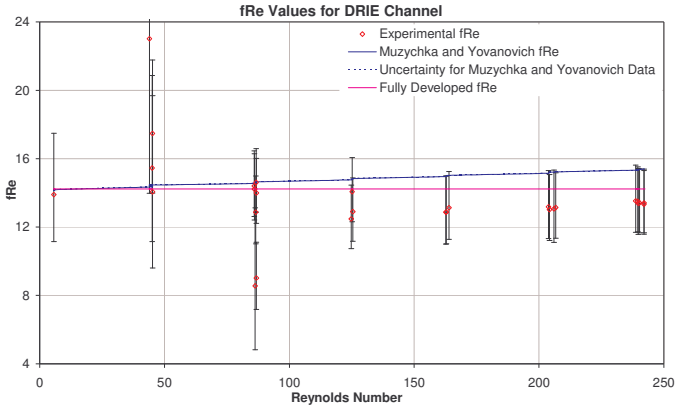

FIGURE 6: FRICTION FACTOR TIMES REYNOLDS NUMBER DATA FOR DRIE CHANNELS. POINTS AT *Re* = 5.7, *fRe* = 63.7 AND *Re* = 6.1, *fRe* = 26.6 HAVE NOT BEEN SHOWN FOR SCALING REASONS.

Figure 6 and Figure 7 plot the experimental and theoretical friction factor times the Reynolds number as calculated for each experimental point against the Reynolds number. It can be seen that the uncertainty in the Muzychka and Yovanovich correlation is very small for this data as Equations (3) and (4) calculate the *fRe* value directly. The uncertainty in the fully developed flow correlation is too small to be visible in the graph. The uncertainty in the experimental data is much higher as *fRe* is derived from the experimental data by working backwards through Darcy's equation and as a result carries more cumulative uncertainty than the theoretical correlations.

Both sets of pressure flow data show experimental values below the expected theoretical values. This was unexpected as previous work using similar channels found an excellent correlation between theory and experiment[6].

It should be noted that the *fRe* data shown in Figure 6 cannot be said to show an experimentally significant deviation from conventional theory as the 95% confidence interval on the DRIE pressure flow measurements shown by the error bars in Figure 6 overlaps with both the fully developed and the developing flow theoretical predictions. The data for the trapezoidal channels in Figure 7 does however indicate an experimentally significant deviation from the theoretical prediction.

This deviation from theory may be related to the use of an optical microscope to measure the channels rather than the scanning electron microscope used in the previous work. Due to the limited depth of field available to an optical microscope, it is possible that the measurements overestimated the size of the channel based on only being able to look at the surface of the channel inlet. Since P_L is proportional to $1/D_h^4$, an error of 1% in the channel measurement will cause an error of the order of 4% in the theoretical pressure drop.

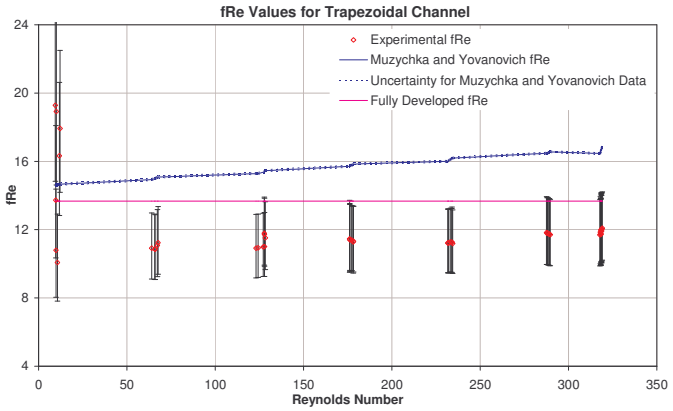

FIGURE 7: FRICTION FACTOR TIMES REYNOLDS NUMBER DATA FOR TRAPEZOIDAL CHANNELS. ONE POINT AT *Re* = 9.6, *fRe* = 38.9 HAS NOT BEEN SHOWN FOR SCALING REASONS.

Heat transfer data

The heat transfer measured from the channels was quite unexpected. Both the DRIE and wet etched channels showed a very strong linear relationship between the Reynolds number and the Nusselt number once the manifold heating effect was accounted for. The Nusselt number results for the wet etched channels in Figure 9 in particular show very high linearity, while the DRIE data in Figure 8 also shows a strongly linear trend for the experimental data based on the Muzychka and Yovanovich correlation[13], while there is more scatter including 9 points that remain negative in the experimental data based on using fully developed correlations to account for the manifold heating effect.

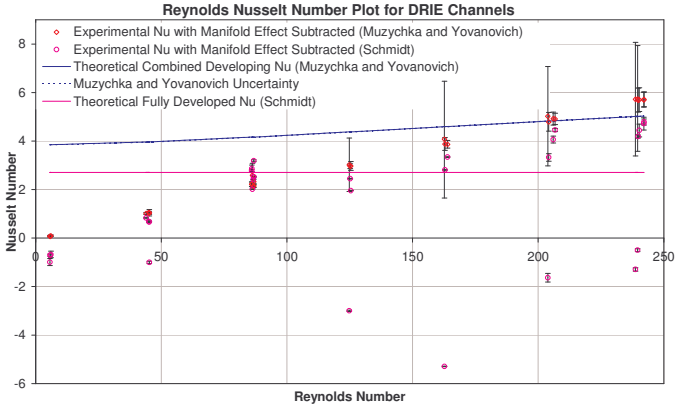

FIGURE 8: REYNOLDS - NUSSELT PLOT FOR DRIE CHANNELS.

A practical limit with the test system used for this work is that instrumentation cannot be fitted to measure the fluid and surface temperatures along the channel due to the sealed nature of the channel samples. Work such as that by Tiselj et al[18] and Li et al[11] correlated low Reynolds number experimental heat transfer data with numerical simulations and found that the assumption made for this work of a constant temperature

gradient through a channel can be invalidated in the case of microchannels with walls which are thick relative to their flow area, cut in thermally conductive substrates. The effect of the manifold heat transfer manifested strongly in this work also. It would still be expected that measured data should follow similar trends to the established correlations however.

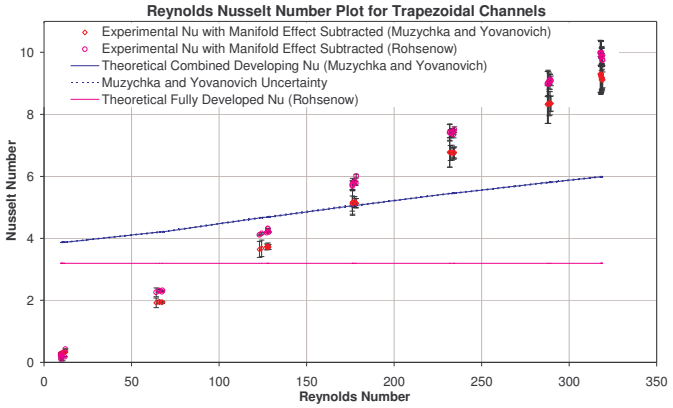

FIGURE 9: REYNOLDS - NUSSELT PLOT FOR WET ETCHED CHANNELS.

Where axial conduction is significant in a flow channel, Nusselt numbers are generally lower than expected, but for this data the linear trend exceeds the upper limits of the theoretical data at high *Re* values while starting from well below these limits.

Since a number of correlations for the Nusselt number include the Reynolds number raised to a various powers, a survey of available literature looking for a linear dependence of the Nusselt number on the Reynolds number was conducted. The highest power to which the Reynolds number is raised in a Nusselt number correlation is 1.17, in the case of a correlation suggested for laminar flow in 1991 by Choi et al[4]. This is given in Equation (9). While this predicts a more rapid increase in the Nusselt number with Reynolds number than the current experimental measurements show, the experimental Nusselt numbers are over five times as large as those predicted using this correlation.

$$Nu_{Choi} = 0.000972\, Re^{1.17}\, Pr^{1/3} \tag{9}$$

It is interesting to note however that the turbulent correlation for the Nusselt number in round tubes based on the Colburn analogy, given in Equation (10), matches very well with the DRIE channel data, though this appears to be coincidence rather than correlation as it is about 50% lower than the trapezoidal channel data. It must be noted however that based on the pressure flow data there is no evidence of a transition to turbulent flow in the system, so the use of this correlation is questionable in any case.

$$Nu_{Colburn} = 0.04\, Re^{0.75}\, Pr^{1/3} \tag{10}$$

Surface roughness was not measured for the channels tested. This may contribute to the unusual results however, it was recently shown in [11] that pressure flow data from smooth walled fused silica microtubes correlated well with theory, while rougher walled steel tubes gave a slightly higher pressure drop. If roughness was to blame for the unusual heat transfer data described in this work, a higher pressure drop than would be expected from theoretical predictions would have been measured rather than a lower one.

It must be concluded from this then, that the effect seen here is likely to have been caused by axial conduction in the channel walls tested rather than being as a result of experimentally new behaviour in the microchannels. Numerical modelling of this system will be performed in order to confirm this hypothesis by predicting the experimental data numerically.

CONCLUSIONS

- The *fRe* values from the system are less than predicted by both developing and fully developed theory. Though the DRIE channel data does not show an experimentally significant deviation from theory, this is still unexpected as previous pressure flow work on similar channels[6] correlated extremely well with theory. The use of limited depth of field optical microscope rather than a scanning electron microscope in measuring the channels may be the cause of this effect.
- Accounting for the effect of manifold heating on the heat transfer from the channel is essential to the correct interpretation of the heat transfer data from the system.
- The Nusselt number measured for this work shows a strong linear dependence on the Reynolds number.
- Numerical simulation of the test system will be performed in order to conclude as to the validity of the Nusselt number data.

ACKNOWLEDGMENTS

The authors gratefully acknowledge the support of Science Foundation Ireland (SFI), IDA Ireland and Bell Labs through the Centre for Telecommunications Value-Chain Research (CTVR) Programme www.ctvr.ie.

REFERENCES

[1] Bavière, Roland, Michel Favre-Marinet, Stéphane Le Person, 2006, "Bias effects on heat transfer measurements in microchannel flows", International Journal of Heat and Mass Transfer, 2006, Article in Press.

[2] Bejan, A., 2000, Shape and Structure, From Engineering to Nature, Cambridge University Press, Cambridge, UK.

[3] Çengel, Yunus A., 1998, Heat Transfer A Practical Approach, International Edition, WCB McGraw-Hill.

[4] Choi, S.B.; R.F. Barron, R.O. Warrington, 1991, "Fluid flow and heat transfer in microtubes", Micromech. Sensors Actuat. Syst. ASME DSC 32 (1991) 123–134.

[5] Eason, C., T. Dalton, C. O'Mathúna, O. Slattery, M. Davies, 2005. "Direct Comparison Between Five Different Microchannels, Part 1: Channel Manufacture and

Measurement", Heat Transfer Engineering, 26(3):79-88, Taylor and Francis Inc.
[6] Eason, C., T. Dalton, C. O'Mathúna, O. Slattery, M. Davies, 2005. "Direct Comparison Between Five Different Microchannels, Part 2: Experimental Description and Flow Friction Measurement", Heat Transfer Engineering, 26(3):89-98, Taylor and Francis Inc.
[7] Eason, Cormac, 2005, "Measurement of Pressure Drop and Heat Transfer Analysis of Microchannels", PhD Thesis, University of Limerick, Ireland.
[8] Garimella, Suresh V., 2006, "Advances in mesoscale thermal management technologies for microelectronics", Microelectronics Journal 37 (2006) 1165-1185
[9] Judy, J.; D. Maynes, B. W. Webb, 2002. "Characterization of frictional pressure drop for liquid flows through microchannels", International Journal of heat and mass transfer 45 (2002) 3477-3489.
[10] Lee, P.S., S.V. Garimella, 2006, Thermally developing flow and heat transfer in rectangular microchannels of different aspect ratios", International Journal of Heat Transfer, article in press.
[11] Li, Zhou; Ya-Ling He, Gui-Hua Tang, Wen-Quan Tao, 2007, "Experimental and numerical studies of liquid flow and heat transfer in microtubes", International Journal of Heat and Mass Transfer (2007), Article in Press.
[12] Muwanga R., I. Hassan, 2006, "Local Heat Transfer Measurements in Microchannels Using Liquid Crystal Thermography: Methodology Development and Validation", Journal of Heat Transfer, July 2006, Vol. 128, pp. 617-626.
[13] Muzychka, Y. S. and M. M. Yovanovich, 2004. "Laminar Forced Convection Heat Transfer in the Combined Entry Region of Non-Circular Ducts", Journal of Heat Transfer, Transactions of the ASME, February 2004, Vol. 126, pp. 54-61.
[14] Rohsenow, W.M., J.P. Hartnett, E.N. Ganić, (ed.), 1985, Handbook of Heat Transfer Fundamentals, 2nd Edition, McGraw-Hill Book Company.
[15] Schmidt, F. W., presented in Shah, R. K. and A. L. London, 1978, "Laminar Flow Forced Convection in Ducts", Academic, New York, 1978.
[16] Shen, S., J.L. Xu, J.J. Zhou, Y. Chen, 2005, "Flow and heat transfer in microchannels with rough wall surface", Energy Conversion and Management 47 (2006) 1311-1325.
[17] Steinke, Mark E., Satish G. Kandlikar, 2006, "Single-phase liquid friction factors in microchannels", International Journal of Thermal Sciences, article in press.
[18] Tiselj, I; G. Hetsroni, B. Mavko, A. Mosyak, E. Pogrebnyak, Z. Segal, 2004, "Effect of axial conduction on the heat transfer in micro-channels", International Journal of Heat and Mass Transfer 47 (2004) 2551-2565.